GEOMETRIC CALIBRATION AND ORTHORECTIFICATION OF BILSAT–1 IMAGERY

Ali Özgün Ok, Res. Assist. *
Mustafa Turker, Assoc. Prof. **
*Geodetic and Geographic Information Technologies
Middle East Technical University, Ankara, Turkey 06531
** Hacettepe University, Faculty of Engineering,
Department of Geodesy and Photogrammetry,
06800 Beytepe, Ankara, Turkey
oozgun@metu.edu.tr
mturker@hacettepe.edu.tr

ABSTRACT

A physical model, which was developed for the orthorectification of the BILSAT–1 Multispectral (XS) imagery, is presented. To model the physical reality of the BILSAT–1 sensor, the well known collinearity condition equations are utilized. The developed model was tested using three study areas. The accuracies of the orthorectified BILSAT–1 images were evaluated with and without using the self-calibration parameters in order to evaluate the significance and the necessity of integrating the self-calibration parameters during the orthorectification process. The Ground Control Points (GCPs) were collected using 1:25,000- scale topographic maps. It was found that, the physical model provides RMS error values less than one pixel for the GCPs and around one pixel for the independent check points (ICPs) when the self-calibration parameters are involved during the orthorectification process. The results also confirm that without using the self-calibration parameters, the RMS error values of less than one pixel is not guaranteed for the orthorectified BILSAT–1 imagery.

INTRODUCTION

BILSAT–1 satellite was successfully launched on September 27, 2003. It is a 129 kg micro-satellite orbiting in a circular sun-synchronous low Earth orbit, at an altitude of 686 km. The major satellite payloads consist of 12.6 meter panchromatic and 27.6 meter 4 channel multispectral sensors. In addition, a low resolution multispectral (8-band) R&D camera (COBAN) and a real time JPEG2000 image compression DSP card (GEZGIN) both developed by Turkish engineers are also accommodated on the satellite (Bradford et. al., 2002). The panchromatic and multispectral sensors have a CCD frame of 2048x2048 pixels and provide 8 bit data (Yuksel et. al., 2004). The satellite provides stereoscopic images as a result of its three-axis control mode, which gives satellite the ability to rotate about any defined axis up to +/- 30 degrees. This property of the satellite gives opportunity to acquire off-track images, which reduces the revisit time of the satellite to approximately 4 days. The technical specifications of the BILSAT–1 and its onboard sensors are given in Table 1.

Table 1. The technical specifications of the BILSAT–1 sensors

Parameter	**Specification**		
Orbital path	Circular - Sun-synchronous		
Orbital period	97.7 min		
Altitude	686 km		
Inclination	98°		
Revisit time	4 days (XS) - 5 days (PAN)		
Sensor	**Pan**	**XS**	**R&D**
Pixel size	12.6 m	27.6 m	~ 80 m
Swath width	25x25 km	55x55 km	51x38 km
CCD size	2048x2048	2048x2048	640x480
Quantization	8 bit	8 bit	8 bit
Number of bands	1	4	8

BILSAT–1 is a member of DMC (Disaster Monitoring Constellation), which is an international partnership led by SSTL, and comprises a network of five small satellites and ground stations (DMC Constellation, 2005). This constellation enables monitoring and delivery of satellite data concerning disasters occurred wherever on Earth and offers daily images at the equator and several imaging opportunities per day at higher altitudes. As a result, the DMC

Consortium formed the first-ever micro-satellite constellation bringing remarkable Earth observation capabilities both nationally and internationally.

This study presents the geometric calibration and orthorectification of BILSAT–1 multi-spectral (XS) imagery. The radiometric calibration of the panchromatic camera has not been performed yet. For this reason, in the present case, the geometric calibration and orthorectification operations are carried out using the images acquired by the multispectral cameras only. To investigate the accuracy of the geometric calibration and orthorectification of BILSAT–1 multi-spectral scenes, the tests were carried out using three different sites that were selected in Turkey.

DIFFERENT SENSOR MODELING APPROACHES

The images that are collected by different platforms and sensor systems contain various geometric distortions. The handling and the registration process of these images have generally been approached by employing three different sensor models that are (i) generalized (simple) sensor models, (ii) projective (abstract) sensor models, and (iii) physical (rigorous) sensor models (McGlone, 1996). The logic used for these three models are common, which is that a relation is generated between the object space and the image space. The main distinction between the three models is that each utilizes a different mathematical foundation for relating the object space with the image space. In some cases, the mathematical transformation from one type of model to another is also possible.

Generalized (Simple) Sensor Models

Generalized Sensor Models usually involve mathematical models that are easier to understand. These models neither use nor require information related to the sensor, platform, the Earth, and do not reflect the physical geometry of the distortions (Toutin, 2004). In this respect, the Generalized Sensor Models require simple mathematical models to relate the object space and the image space.

A common form of a simple mathematical model used in this category is based on the Polynomial Functions. These functions can be in different forms (2D or 3D) and/or different degrees (1^{st}, 2^{nd}, 3^{rd} etc.). The special forms of the 3D Polynomial Functions are also available and implemented, as in Pala and Pons (1995). In addition, the Rational Functions, which relate the image space and the object space through a ratio of 3D Polynomial Functions, are also introduced (OGC, 1999; Tao and Hu, 2001; Di et. al., 2003). For the Generalized Sensor Models, the registration accuracy is proportional with the form (type, degree) of the polynomial used and also to the number, the distribution and the accuracy of the input Ground Control Points (GCPs). Therefore, the desired registration accuracy is hardly achieved using these models. Moreover, the potential correlations between the parameters inside the higher order Generalized Sensor Models might result in an unstable model solution. However, despite these problems, the simplicity in their implementation makes the Generalized Models attractive to the researchers and users.

Projective (Abstract) Sensor Models

These models are based on projective geometry that allows simple representations of the objects and their images to facilitate theoretical analysis (Mahapatra et. al., 2004). The Abstract Sensor Models involve the Projective Transformation (PT) and Direct Linear Transformation (DLT). Similar to the Generalized Models, the information related to the sensor and the platform is not required to solve the parameters of the Abstract Sensor Models. Alternatively, this information is implicit in the parameters and the transformation from the PT parameters to the sensor parameters is possible (Kobayashi and Mori, 1997).

The modified forms of the Abstract Sensor Models are also used. For those satellite sensors that use line perspective relationship between the image space and the object space such as SPOT, the use of the modified version of PT is recommended (Novak, 1992). A modified version of the DLT, which was developed by El-Manadili and Novak (1996), can also be applied to the push-broom sensors. However, similar to the Generalized Models, the Abstract Sensor Models also suffer from achieving the desired registration accuracies when the number of GCPs is not high and are not well distributed throughout the study area.

Physical (Rigorous) Sensor Models

A physical model is a complex model which uses the physical reality of the sensor by integrating the knowledge of the ephemeris and attitude data. Several physical models have been developed and considerable research has been carried out. However, for all the developed physical models, the milestone is the very well known photogrammetric collinearity equations. The parameters inside the collinearity equations can be divided into two categories that are

namely the interior and the exterior orientation parameters. While the interior orientation defines the sensor characteristics required for the reconstruction of the object space bundle of rays from the corresponding image points, the exterior orientation establishes the position and orientation of the bundle rays with respect to an object space coordinate system (Mikhail et. al., 2001).

The interior orientation parameters are usually determined prior to the launch of the satellite during a laboratory calibration process. However, the interior orientation may change during the launch and/or in the orbit. Therefore, it must be calibrated and validated from time to time (Jacobsen, 2006). Depending on the sensor type (frame or linear), the exterior orientation of an image can be fixed or dynamic and it can be determined along with the Global Positioning System (GPS), star sensor, sun sensors, or gyros. However, both the interior orientation control during the post-flight calibration and the precise exterior orientation determination processes require well defined GCPs on the acquired images and the parameter estimation procedure. Because of the constitution of the physical foundation of the image acquisition, the number of GCPs required to solve the physical sensor models is less than the number of GCPs to solve the simple and abstract sensor models. Thus, the registration accuracies achieved from the physical sensor models becomes quite high even for the parts where the GCPs are not available.

Until now, many works have been published related to the physical sensor models. All these models tried to achieve the best image registration accuracies for various sensors onboard different platforms by integrating the main advantages of the physical models, high precision and robustness. On the other hand, the main disadvantage of the all developed physical models is their computational complexities during the implementation.

MODEL DEVELOPMENT

BILSAT–1 is equipped with four sun sensors, four rate sensors, two magnetometers, two star cameras, and a SGR-10 GPS receiver to accomplish the advanced knowledge of the attitude and position information. Prior to the launch of the satellite, the satellite is estimated to have an attitude control accuracy of ±0.02 deg., an attitude knowledge of ±0.006 deg., and an orbital position knowledge of ±50 m (Bradford et. al., 2002). However, after the launch of the satellite, the problems occurred with the star cameras and, for the time being, the attitude information of the images acquired is obtained from the sun sensors only. Therefore, the knowledge of the accuracy of the attitude decreased dramatically. The actual performance of the onboard GPS receiver is also an open question after the launch of the satellite.

Figure 1. BILSAT–1 XS cameras (Yuksel et. al., 2004).

The multispectral image acquisition of BILSAT–1 is performed using four separate cameras (NIR, R, G, and B), which are arranged in a contiguous form (Fig 1). Therefore, each camera is physically separated (modular camera approach) and has its own physical configuration. Unfortunately, the pre-flight laboratory calibration of the cameras was not performed. For this reason, the interior orientation parameters of the cameras are not available. Moreover, for the time being, the payload geometrical information is also not available.

Based on the above information, a high quality direct registration control should not be expected from the BILSAT–1 sensors. It becomes therefore, quite necessary to develop a physical sensor model, which is strictly supported by the GCPs (indirect registration) to recover the exterior orientation parameters of BILSAT–1. Then, it will become possible to recover the interior orientation parameters of the developed sensor model via the additional parameters (APs). After recovering the interior and the exterior orientation parameters, the initial attitude and the position information can be compared with the results obtained from the indirect registration. Thus, the direct registration capabilities of BILSAT–1 sensors can be addressed.

BILSAT–1 acquires the multispectral images as the snapshots using a 2048x2048 pixel frame CCD array. Because a frame sensor acquires the whole image at an instant of time, for each image, the exterior orientation parameters will become fixed. Thus, the regular collinearity conditions and a rotation matrix can be used to relate the image space and the object space (1 and 2) without any modification (Manual of Photogrammetry, 2004).

$$x - x_0 = -f\frac{R_1}{R_3} = F_1$$
$$y - y_0 = -f\frac{R_2}{R_3} = F_2 \quad (1)$$

where;

$$\begin{bmatrix} R_1 \\ R_2 \\ R_3 \end{bmatrix} = R \times \begin{bmatrix} X - X_L \\ Y - Y_L \\ Z - Z_L \end{bmatrix} \quad (2)$$

In above equations, x, y are the image space coordinates of a point, X, Y, and Z are the object space coordinates of the same point, X_L, Y_L, Z_L are the object space coordinates of the perspective centre, f is the focal length of the sensor, x_0 and y_0 are the coordinates of the principal point, and R is the rotation matrix that represent the ω, φ, κ rotations of the image coordinates with respect to the ground coordinates (3):

$$R = \begin{bmatrix} \cos\varphi\cos\kappa & \cos\varphi\sin\kappa & \sin\omega \\ \sin\omega\sin\varphi\cos\kappa + \cos\omega\sin\kappa & -\sin\omega\sin\varphi\sin\kappa + \cos\omega\cos\kappa & -\sin\omega\cos\varphi \\ -\cos\omega\sin\varphi\cos\kappa + \sin\omega\sin\kappa & \cos\omega\sin\varphi\sin\kappa + \sin\omega\cos\kappa & \cos\omega\cos\varphi \end{bmatrix} \quad (3)$$

Equation 1 assumes perfect conditions for relating image space with the object space. However, there may be systematic errors that may arise from a number of sources during the imaging process (Manual of Photogrammetry, 2004). These systematic errors can be removed by introducing the additional parameters (APs) to the collinearity equations (Novak, 1992; Fraser, 1997; Habib et. al., 2002; Manual of Photogrammetry, 2004; Jacobsen, 2006). The inclusion of the APs to the collinearity model extends the model as shown in equation (4), where Δx and Δy represent the image coordinate correction functions.

$$x - x_0 + \Delta x = -f\frac{R_1}{R_3}$$
$$y - y_0 + \Delta y = -f\frac{R_2}{R_3} \quad (4)$$

In the past studies, a number of mathematical models have been proposed to find the best parameter configuration of the APs. The AP models can be divided into three categories, among which the most widely used and the accepted one is the physical AP model. This model seeks the most appropriate parameters to compute the correction functions of the image coordinates based on four principal sources of distortions from the collinearity, which are physically interpretable. These distortions include the symmetric radial distortion, decentering distortion, image plane unflatness and in-plane image distortion (Fraser, 1997). At any point, the net image displacement will amount to the cumulative contribution of each of these distortions (Manual of Photogrammetry, 2004). Thus, this image displacement can be represented as follows (5):

$$\Delta x = \Delta x_r + \Delta x_d + \Delta x_u + \Delta x_f$$
$$\Delta y = \Delta y_r + \Delta y_d + \Delta y_u + \Delta y_f \quad (5)$$

where, the subscript r stands for radial distortion, d represents decentering distortion, u represents image plane unflatness, and f represents in-plane distortion. The sources and the formulation of each distortion are well explained

in Fraser (1997), Manual of Photogrammetry (2004), and Poli (2005). In the present case, only the complete self-calibration model including the corrections to the interior orientation parameters is given in equation (6).

$$\begin{aligned}\Delta x &= -x_0 - \frac{\bar{x}}{f}\Delta f + \bar{x}r^2K_1 + \bar{x}r^4K_2 + (2\bar{x}^2 + r^2)P_1 + 2P_2\bar{x}\bar{y} - A_1\bar{x} + A_2\bar{y} \\ \Delta y &= -y_0 - \frac{\bar{y}}{f}\Delta f + \bar{y}r^2K_1 + \bar{y}r^4K_2 + (2\bar{y}^2 + r^2)P_2 + 2P_1\bar{x}\bar{y} + A_1\bar{y}\end{aligned} \tag{6}$$

where;

$$r^2 = \bar{x}^2 + \bar{y}^2 = (x - x_0)^2 + (y - y_0)^2$$

In equation (6), f is the focal length of the sensor, x_0 and y_0 are the coordinates of the principal point, Δf represents a correction to the focal length, K_1 and K_2 stand for the symmetric radial lens distortion, and P_1 and P_2 are the decentering distortion parameters. The last two terms A_1 and A_2 introduce the in-plane distortions that are designed in a way to eliminate the correlations between other APs (Habib et. al., 2002).

As mentioned earlier, the distortions can be removed by introducing the additional parameters (APs) to the collinearity equations and the results can reveal significant accuracy improvements when the APs are introduced. However, in some cases, the level of distortion to be modeled in the physical models may not reflect a substantial increase in terms of the required level of accuracy. For instance, the lens distortion is often neglected for the modern mapping cameras since its magnitude is usually not more than a few micrometers (McGlone, 1996). Therefore, in this study, the accuracy of the orthorectification of the BILSAT–1 XS images is tested using both with and without introducing the APs in the physical model.

THE IMPLEMENTATION OF THE MODEL

To implement the physical model, a program was developed using MATLAB® v. 6.5. The developed program can serve as a base geometric model for BILSAT–1 sensor and can be characterized for the future missions. Initially, the program imports the GCPs, which are referenced to the UTM projection and WGS-84 datum. However, from the photogrammetric point of view, the UTM projection cannot be used due to the scale changes inherent for the horizontal components. As is well known, the collinearity conditions require an orthogonal coordinate system. The geocentric coordinate system is orthogonal. However, it is not favorable for data handling – the original horizontal and the vertical coordinate components are mixed. Therefore, it becomes difficult to use the correct weights for different accuracy in the original coordinate components (Jacobsen, 2002). For this reason, in the present case, the Local Space Rectangular (LSR) coordinate system was employed in the developed program. To employ the LSR coordinate system, a transformation is needed to be carried out from the UTM projection system to the LSR coordinate system. The transformation contains three successive coordinate transformations that are (i) from UTM to Geodetic, (ii) from Geodetic to Geocentric, and (iii) from Geocentric to LSR. Thus, all these transformations were performed using the equations given and explained in Mikhail et al (2001). Similarly, the transformations from LSR coordinate system to UTM projection system were also carried out in the reverse order.

The LSR orthogonal coordinate system is a right-handed system with an arbitrary origin (Manual of Photogrammetry, 2004). For the transformation from geocentric to LSR coordinate system, first GCP point in each GCP dataset is used as the origin (Jacobsen, 2005). Similarly, the initial coordinates of the positional exterior orientation parameters are referenced to the geocentric coordinate system and they are also converted to the LSR orthogonal coordinate system with the same origin. In the present case, each step of the transformation was carefully examined and the results of each transformation were compared with the results obtained using the independent geographic translator – GEOTRANS, which is distributed by NGA (NGA, 2006). The results of the comparison revealed that there were no differences between the results of the developed program and the results of GEOTRANS.

Next, the well known least squares estimation method was used to estimate the unknown parameters of the physical model. Apparently, in the physical model, the relation between the parameters and the observations were non-linear. Therefore, the linearization process was performed. Similar to the study conducted by Poli (2005), the exterior and interior orientation parameters were estimated independently. First, the exterior orientation parameters were estimated. To do that, for each image, the initial values were taken from the imaging survey files. These files

contain the entire information related to the orientation and the position of the satellite on the day of image acquisition. Second, the interior orientation parameters were estimated by fixing the exterior orientation parameters that were estimated previously. For all the interior orientation parameters, the initial values were set to zero and the value of the initial focal length was taken to be 180 mm. During the estimation procedure, the values of the parameters were used to compute, iteratively, the new approximate values. In each iteration, the computed new approximate values were used to compute the partial derivatives that were essential for the linearization. The iterations were carried out until the differences between the values of the successive iterations become sufficiently low. The difference was tested by means of a convergence value, which was defined as 10^{-5} in this study. The results revealed that this condition was excessively satisfied in the fifth and second iterations of the estimations for the exterior and interior parameters, respectively.

DATA SETS

BILSAT–1 XS Image Datasets

Three BILSAT–1 XS images selected in different parts of Turkey were used to test the accuracies of the orthorectified images. The characteristics of each study area and their corresponding BILSAT–1 XS datasets are as follows:

- The study area covered by the image "20040730073227_171" (36°33´N, 33°13´ E – image center) is located in the southern part of Turkey (Figure 2d). It is approximately 70 km southern part of the city of Cankiri. In the area, the elevation ranges from approximately 70 m for the flat areas to over 2010 m in the high mountains to the north-west, providing a total relief in excess of approximately 1940 m. For this area, the BILSAT–1 XS image (approximately 57 x 57 km) was acquired in July 2004.
- The study area covered by the image "20040804072344_207" (41°28´N, 33°48´ E – image center) is located in the northern part of Turkey (Figure 2c). The city of Kastamonu falls within the area, where the terrain elevation ranges from approximately 560 to 1940 m. For this area, the BILSAT–1 XS image (approximately 55 x 52 km) was acquired in August 2004.
- The study area covered by the image "20050626081629_2241" (37°24´N, 27°41´ E – image center) is located in the south-western part of Turkey (Figure 2b). The area covers a part of the gulf of Gulluk. While the Lake Bafa lies in the north-western part, the city of Aydin is situated approximately 46 km northern part of the area. The elevation ranges from the sea level to over 1420 m. For this area, the BILSAT–1 XS image (approximately 78 x 63 km) was acquired in June 2005.

As stated earlier, the BILSAT–1 XS sensor uses a modular camera approach and the cameras are physically separated. Therefore, each camera may have different physical and/or radiometric characteristics. Due to this reason, in this study, the camera that has the best radiometric characteristics was chosen. After an extensive visual inspection, the camera for the green band of the BILSAT–1 XS images was found to be the most satisfying layer in terms of the radiometry. Therefore, for each study area, the green layer of the BILSAT–1 XS images was selected and the geometric calibration and the orthorectification procedures were carried out using the images of green layer. Once the geometric calibration and the orthorectification of the green layer image are performed then, the remaining layers can be easily transformed using the green image as the base and by means of the 7–parameter (scale, rotation, translation) transformation.

In addition to the image data, for each image, an imaging survey file that contains the entire information related to the orientation and the position of the satellite on the day of acquisition was appended. Thus, the approximate orientation and the position information of the satellite during the image acquisition were available. The names of the image files, which are originally distributed, are too long to be used in this paper. Henceforth, each image is termed as only with the numbers placed at the right part of the under-slash operator in the original file names.

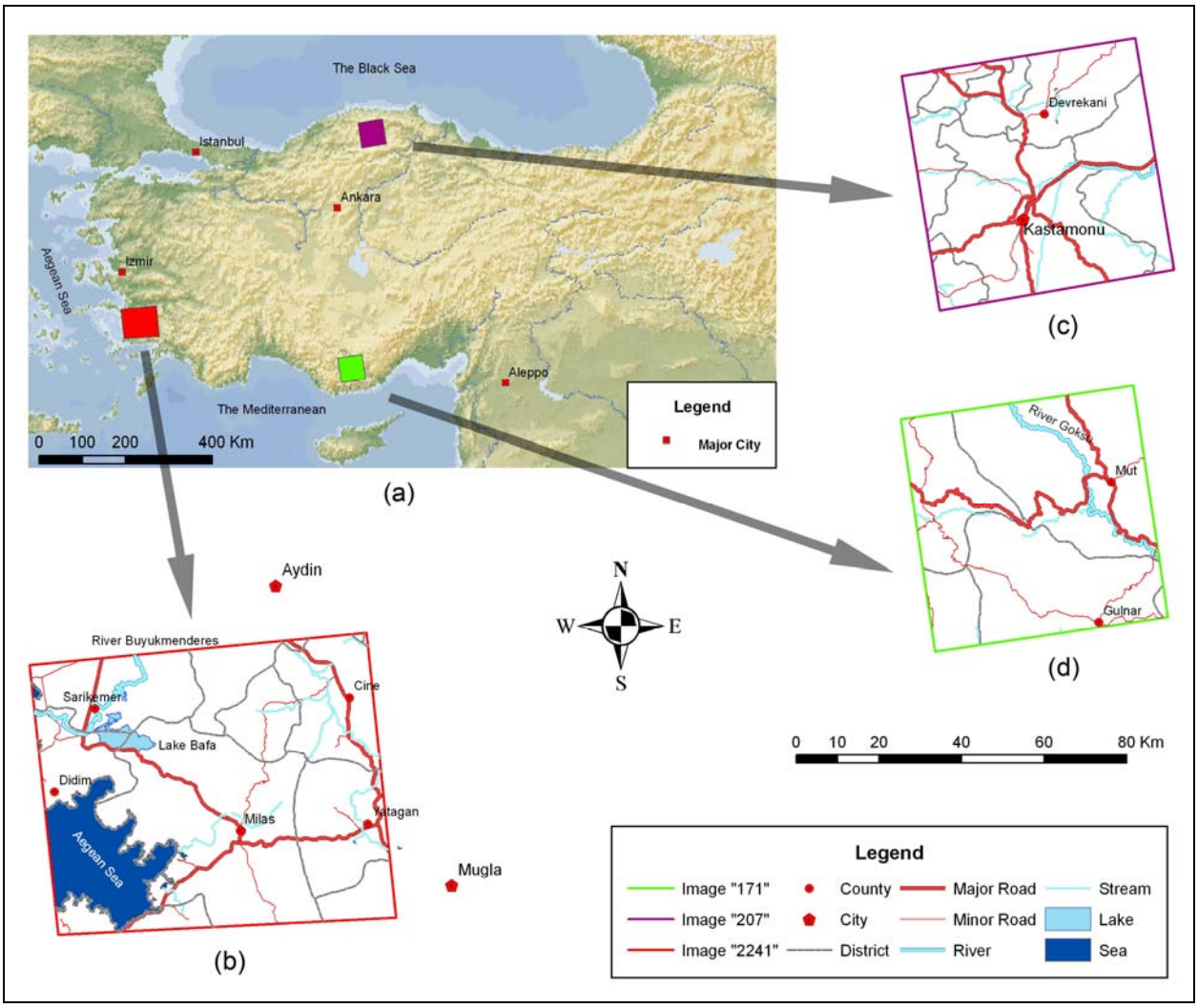

Figure 2. The study area. (a) The overall scene of the study areas, (b) the study area of image "2241", (c) the study area of image "207", and (d) the study area of image "171".

Reference and GCP Datasets

A total of 121 1:25,000- scale digital topographic maps covering the three test sites were available. The topographic maps were produced by the General Command of Mapping of Turkey. The General Command of Mapping is a national mapping agency of Turkey that is in charge of the production and revision of 1:25,000- and smaller-scale topographic maps which were compiled with to NATO level A standards. Most of the topographic maps that were used in this study have not been revised for about fifteen years and are referenced to the Universal Transverse Mercator (UTM) projection and European Datum 1950 (ED50). The average planimetric accuracy (σ_X, σ_Y) of the 1:25,000 scale topographic maps are stated to be ±5 meters (HGK, 2007). The digital topographic maps were registered using the Orthoengine® module of PCI Geomatica v. 10.00 image processing software. To register the digital topographic maps, the second order polynomial rectification method and the nearest neighbor interpolation method were used. At least 12 evenly distributed points were used during the registration and only those maps with an overall RMSE less than 1 pixel size (≈ 3,04 m) were accepted. For those maps that did not meet the 1 pixel-size accuracy level, either the existing points were recollected and/or new points were added. As a result, for all available digital topographic maps, the final registration accuracy was estimated to be better than ±3 m.

Next, the elevation reference dataset was prepared from the contour lines of the digital 1:25,000-scale topographic maps. The elevation values of the digital contour lines were referenced to the mean-sea level and estimated to have a vertical accuracy (σ_Z) of ±2.5 meter (HGK, 2007). To generate a grid DEM from digital contour lines, a large variety of interpolation algorithms has been proposed or developed (Carrara et. al., 1997). In this study,

for each test site, the ICP elevation reference grid DEMs were generated using the Orthoengine™ module of PCI Geomatica. This module uses the "Finite Difference" interpolation method to generate the grid DEMs and performs the interpolation in three steps. In the first step, the vector elevation values are assigned into the corresponding pixels in grid DEM. In the second step, the elevations for the remaining pixels are interpolated using the Distance Transform algorithm, which estimates the values from those pixels equidistant from the pixels assigned in the first step. In the last step, the "Finite Difference" algorithm iteratively smoothes the grid DEM (Orthoengine User Guide, 2003).

Table 2. The interpolation errors of the reference DEMs

Study Area	Elevation Test Points	Errors (m)	
		Average Error	Standard Error
"171"	84,863	-0,1120	±2,17531
"207"	65,397	-0,0561	±1,34513
"2241"	103,891	-0,0859	±1,64845

During the production of grid DEMs interpolation errors occur inherently from digital contour lines. According to the USGS National Mapping Division accuracy assessment standards, a minimum of 28 test points per DEM is required to compute the RMSE, which is composed of a single test using 20 interior points and 8 edge points (USGS, 2004). However, in this study, each generated DEM was evaluated using an extensive number of test points. The standard errors computed revealed that the overall interpolation errors are of between ±1,345 m and ±2,175 m (Table 2).

The 1:25,000-scale topographic maps covering the three test sites were used for collecting the horizontal coordinates of the GCPs. In addition, the elevation values of the GCPs were also obtained from previously generated 1:25,000- scale DEMs. The GCPs were collected using the ERDAS IMAGINE® v. 9.0 image processing software. When collecting the GCPs, each input image and the corresponding parts of the 1:25,000- scale digital topographic maps were simultaneously displayed on the screen. We found that the collection process of the GCPs was quite labor intensive due in part to the 16+ year time difference between the images and the topographic maps. Furthermore, the moderate spatial resolution of the BILSAT–1 XS images also restricted the collection of GCPs. However, despite these difficulties, for each image, a satisfying number of GCPs was successfully collected. For the three test sites, a total of 105 GCPs were collected using the digital topographic maps. Figure 3 depicts, for each test site, the distribution of the collected GCPs.

As stated earlier, the 1:25,000- scale digital topographic maps were referenced to the UTM projection and ED-50 datum. Thus, for all the GCPs derived from the topographic maps, the reference datum was ED-50. However, the developed program accepts only the GCPs that are referenced to UTM projection and WGS-84 datum. Therefore, a datum transformation was applied to convert the GCP coordinates from ED-50 datum to WGS-84 datum. This transformation was also performed in ERDAS IMAGINE® environment. On the other hand, the height values of the GCPs were referenced to the mean-sea level and a transformation concerning the geoidal undulation was carried out using the developed program.

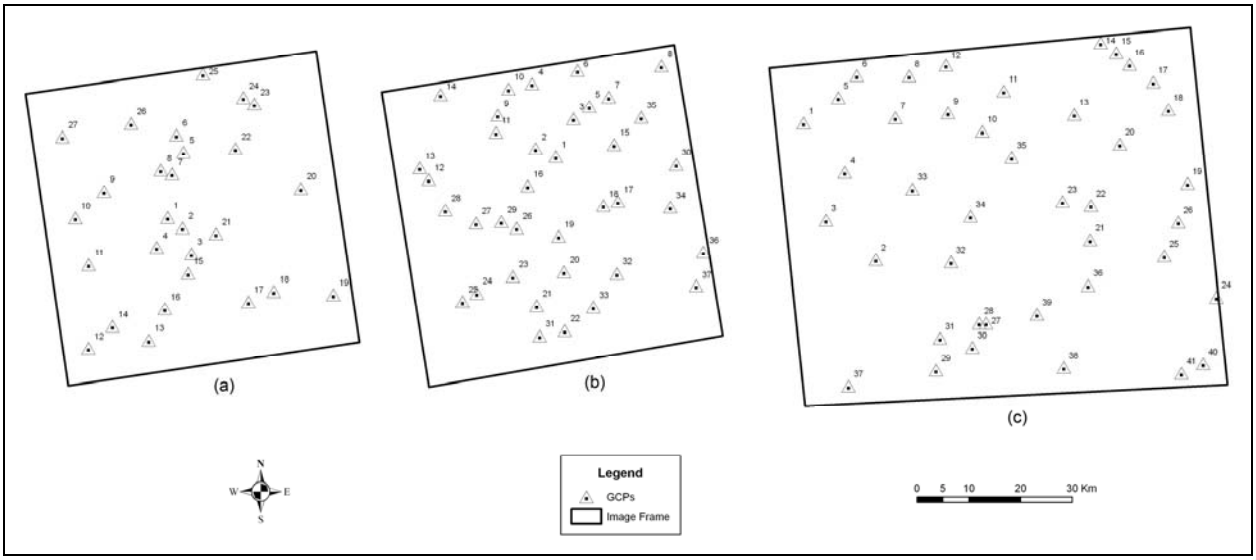

Figure 3. The distribution of the GCPs collected (a) from image "171", (b) from image "207", and (c) from image "2241".

THE RESULTS AND DISCUSSION

Table 3. The results of the physical model for two different sets of GCPs.

Image ID	GCPs / ICPs	GCP RMS Error (pixel)			ICP RMS Error (pixel)		
		X	Y	XY	X	Y	XY
"171"	9 / 18	0.64	0.63	0.90	0.76	0.79	1.10
	27 / -	0.68	0.62	0.92	-	-	-
"207"	9 / 28	0.54	0.44	0.70	0.75	0.89	1.16
	37 / -	0.65	0.69	0.95	-	-	-
"2241"	9 / 32	0.58	0.71	0.92	0.73	0.63	0.97
	41 / -	0.58	0.57	0.81	-	-	-

Table 3 summarizes the results of the RMS error values computed for the control and check points for two different cases. In the first case, 9 evenly distributed points were used to solve the unknowns of the physical model and the remaining points were accepted to be the check points. As can be seen in Table 3, when nine control points are used, the RMS errors were computed for the control points, in *X* and *Y* directions (ΔX and ΔY), in the range of 0.44 and 0.71 pixels, respectively. For the control points, the worst overall RMS error (XY) was computed to be 0.92 pixels. For the check points, a reliable indication of the orthorectification process was given by the RMS errors computed. As can be observed in the last column of Table 3, for check points, the physical model provided the RMS errors around one pixel. The errors of the check points confirm the robustness of the physical model used for the BILSAT–1 XS sensor. In the second case, in which all the points were used as control points, all the RMS errors (XY) were computed to be less than one pixel size of the BILSAT–1 XS image.

Table 3 illustrates the results of all RMS errors that were obtained in the condition where APs are introduced in the physical model. Therefore, for each study area, the computed RMS errors were the possible lowest errors. However, in order to fully understand the effect of APs, which were introduced in the physical model to the computed RMS errors, a different test was carried out. For each study area, the accuracy of orthorectification was tested using (i) with and (ii) without introducing the APs in the physical model. The results of this additional test are given in Table 4, where for the images

Table 4. The results obtained using the physical model (with and without APs)
API : Additional Parameters Introduced

Image ID	API	Number of GCPs	RMSE (pixel)			Improvement (pixel)
			X	Y	XY	
"171"	No	27	0.66	0.69	0.95	0.03
	Yes		0.68	0.62	0.92	
"207"	No	37	0.72	0.72	1.01	0.06
	Yes		0.65	0.69	0.95	
"2241"	No	41	0.87	0.80	1.18	0.37
	Yes		0.58	0.57	0.81	

Table 5. The results of geometric calibration of the exterior and interior orientation parameters

Calibrated Exterior Orientation Parameters			
Parameter	Image ID		
	"171"	"207"	"2241"
X (m)	35117.449	39782.765	-411475.394
Y (m)	22201.454	17426.114	-49512.994
Z (m)	675892.939	678825.761	660362.146
ω (deg)	-1.88828	-2.42113	2.83461
φ (deg)	2.56450	3.40449	-34.18500
κ (deg)	8.38809	8.78871	9.31990
Calibrated Interior Orientation Parameters			
f (mm)	179.811	179.959	179.616
x_0 (mm) x 10^{-3}	0.194	0.198	-2.196
y_0 (mm) x 10^{-3}	1.263	0.499	3.643
K_1 x 10^{-4}	0.441	-0.152	0.499
K_2 x 10^{-6}	-0.394	0.401	-0.167
P_1 x 10^{-4}	-0.049	-0.122	0.239
P_2 x 10^{-4}	-0.210	-0.119	-0.449
A_1 x 10^{-4}	0.501	-0.265	0.829
A_2 x 10^{-4}	-1.950	1.159	1.340

"171" and "207" slight improvements are observed in the computed RMS errors after introducing the APs in the physical model. When the APs are not introduced in the physical model, the RMS errors of 0.95 and 1.01 were computed for the images "171" and "207", respectively. After introducing the APs in the physical model, the RMS error values of 0.92 and 0.95 were computed. As it is obvious, the improvements in the RMS errors were not significant. However, for the image "2241", a significant improvement (0.37 pixels) was observed in the RMS error. This improvement can only be explained after examining the calibrated exterior orientation parameters of each image. Table 5 summarizes the results of the calibrated exterior and interior orientation parameter of each image. The results of the calibrated position parameter are given in the LSR orthogonal coordinate system in which the least squares estimation procedure was carried out. As can be seen in Table 5, the image "2241" was acquired in a condition of a large incidence angle. On the other hand, the images "171" and "207" are almost acquired in nadir, whereas image "2241" was acquired with an excessive phi (φ) angle of -34.185 degrees. Therefore, it is possible to expect more RMS error improvements for the images acquired with large incidence angles. The results of the calibrated exterior orientation parameters also clarify the larger area coverage (approximately 78 x 63 km) of the image "2241" when compared with the images "171" and "207" (Figures 3 and 4).

Figure 4 depicts the error vectors computed in the case where all points are considered as control points. As can be seen in Figure 4, for all study areas, it is obvious that the systematic distortions do not exist. It is also obvious that the individual GCP errors rarely approach two pixels.

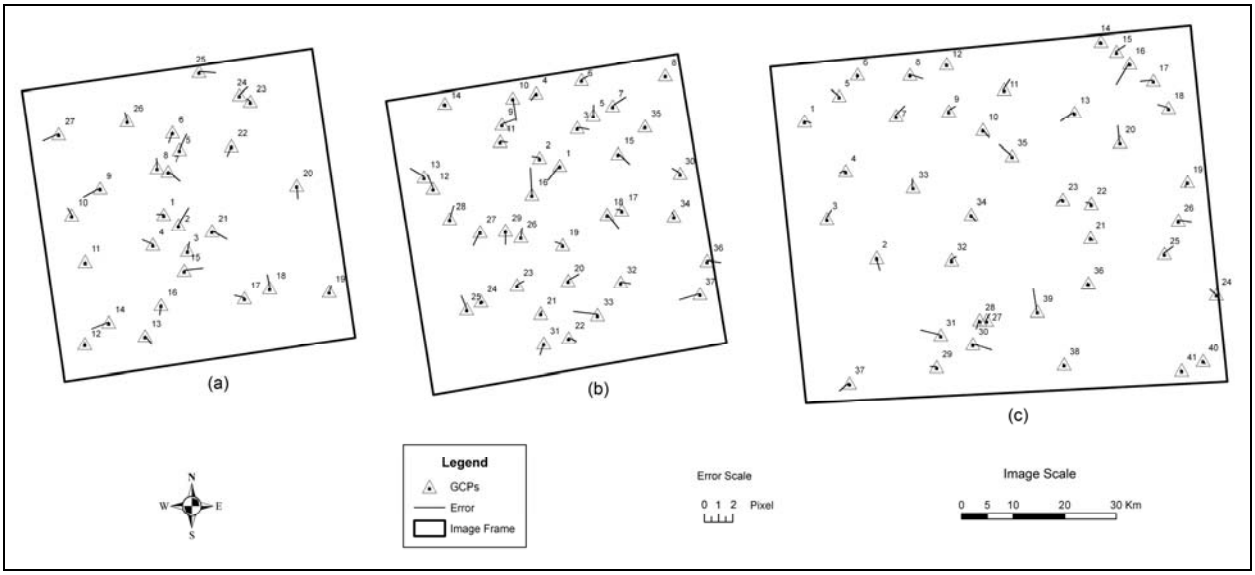

Figure 4. The error vectors for each GCP (a) on image "171", (b) on image "207", and (c) on image "2241".

CONCLUSION

In this study, a physical model, which was developed for the orthorectification of the BILSAT–1 Multispectral (XS) imagery, is presented. To evaluate the developed physical model, three different test sites were used. The GCPs needed to perform the orthorectification process were collected using the 1:25,000- scale digital topographic maps. We found that nine evenly distributed GCPs appear to be sufficient to achieve the orthorectification accuracy around one pixel for the BILSAT–1 XS images. It is reasonable to conclude that, if sufficient number of GCPs are provided, the physical model can produce RMS errors better than one pixel size for the orthorectification of BILSAT–1 XS images.

The tests related to the significance and the necessity of integrating self-calibration parameters during the orthorectification process revealed that the use of self-calibration parameters in the physical model is important. For the control points, the physical model provided accuracies less than one pixel when the self-calibration parameters are included in the model. The results also confirm that without using the self-calibration parameters, the accuracies of less than one pixel is not guaranteed for the orthorectification of the BILSAT–1 imagery. In addition, we found

that, as the incidence angle of the acquired BILSAT–1 XS images gets larger, the self-calibration parameters introduced during the orthorectification process considerably improves the computed RMS errors. Therefore, it is crucial to use the self-calibration parameters for the images acquired with a large incidence angle. Finally, for each study area, the error vectors (Figure 4) revealed that the systematic distortions do not exist and the individual GCP errors rarely approach to two pixels.

The results show that the orthorectification accuracies obtained using a large number of GCPs were better than one pixel size of the BILSAT–1 XS images. However, collection of a large number of GCP may not be possible for most of the BILSAT–1 XS images. Therefore, the developed physical model, which is solved using a small number of GCPs, is capable to orthorectify the BILSAT–1 XS images for those studies that require approximately one pixel accuracy.

ACKNOWLEDGMENTS

The authors would like to thank TUBITAK Space Technologies Research Institute (formerly known as BILTEN) for providing the BILSAT–1 XS images. Especially, the helps of Oktay Algün, Önder Belce, and Ramazan Küpçü during the image data acquisition and handling are gratefully appreciated.

REFERENCES

Bradford, A., Gomes, L. M., Sweeting, M., Yuksel, G., Ozkaptan C., Orlu, U. (2002). BILSAT–1: A Low Cost, Agile, Earth Observation Microsatellite for Turkey. In: *53rd International Astronautical Congress*, Houston, Texas, USA.

Carrara, A., Bitelli, G., Carla, R. (1997). Comparison of techniques for generating digital terrain models from contour lines. *International Journal of Geographical Information Science, 11*(5):451–473.

Di, K., Ma, R., and Li, R. X. (2003). Rational Functions and Potential for Rigorous Sensor Model Recovery. *Photogrammetric Engineering and Remote Sensing, 69*(1):33-41.

DMC Constellation, (2005). DMC International Imaging Ltd., http://www.dmcii.com/products_constellation.htm

El-Manadili, Y., and Novak, K. (1996). Precision Rectification of SPOT Imagery using the Direct Linear Transformation Model. *Photogrammetric Engineering and Remote Sensing, 62*(1):67-72.

Fraser, C. S. (1997). Digital Camera Self-calibration. *ISPRS Journal of Photogrammetry & Remote Sensing, 52*: 149-159.

Habib, A. F., Morgan, M., Lee, Y.R. (2002). Bundle Adjustment with Self-Calibration using Straight Lines. *Photogrammetric Record, 17*:635-650.

HGK, (2007). 1:25,000 Topografik Harita Teknik Ozellikleri, Harita Genel Komutanligi, http://www.hgk.mil.tr/urunler/haritalar/yurticiuretim/topografik/topotek25.html (In Turkish)

Jacobsen, K., (2002). Calibration Aspects in Direct Georeferencing of Frame Imagery. *Int. Arch. Photogramm. Remote Sensing* 34(1): 82 – 88.

Jacobsen, K. (2005). BLTRA User Manual. Institute for Photogrammetry and GeoInformation University of Hannover.

Jacobsen, K. (2006). Calibration of Imaging Satellite Sensors. *Int. Arch. Photogramm. Remote Sensing*. Band XXXVI 1/ W41. Ankara.

Kobayashi, K., and Mori, C. (1997). Relations between the Coefficients in the Projective Transformation Equations and the Orientation Elements of a Photograph. *Photogrammetric Engineering and Remote Sensing, 63*(9):1121-1127.

Mahapatra, A., Ramchandran, R., and Krishnan, R. (2004). Modeling the Uncertainty in Orientation of IRS-1C/1D with a Rigorous Photogrammetric Model. *Photogrammetric Engineering and Remote Sensing, 70*(8):939-946.

Manual of Photogrammetry Fifth Edition (2004). American Society for Photogrammetry and Remote Sensing, ASPRS.

McGlone, C., (1996). Sensor modeling in image registration. *Digital Photogrammetry*. American Society for Photogrammetry and Remote Sensing, Bethesda, Maryland. pp: 115–123.

Mikhail, E. M., Bethel, J. S., and McGlone, J. C. (2001), *Introduction to Modern Photogrammetry*.

NGA, (2006). Geographic Translator (GEOTRANS), National Geospatial Intelligence Agency, http://earth-info.nga.mil/GandG/geotrans/

Novak, K. (1992). Rectification of Digital Imagery. *Photogrammetric Engineering and Remote Sensing, 58*(3):339-344.

OGC – OpenGIS Consortium (1999). The OpenGIS Abstract Specification - Topic 7: The Earth Imagery Case. http://portal.opengeospatial.org/files/index.php?artifact_id=892

OrthoEngine User Guide, (2003). PCI Geomatics.

Pala, V., and Pons, X. (1995). Incorporation of Relief in Polynomial-Based Geometric Corrections. *Photogrammetric Engineering and Remote Sensing, 61*(7):935-944.

Poli, D. (2005). Modeling of Spaceborne Linear Array Sensors. Phd Thesis, Zurich.

Tao, C. V., and Hu, Y. (2001). A Comprehensive Study of the Rational Function Model for Photogrammetric Processing. *Photogrammetric Engineering and Remote Sensing, 67*(12):1347-1357.

Toutin, T., (2004). Review Article: Geometric Processing of Remote Sensing Images: Models, Algorithms and Methods. *International Journal of Remote Sensing, 25*(10):1893-1924.

USGS (2004), Standards for Digital Elevation Models, Part 2 – Specifications, USGS National Mapping Program Technical Instructions.

Yuksel, G., Belce, O., Urhan, H., Gomes, L., Bradford, A., Bean, N., Curiel, A. S. (2004). BILSAT–1: First Year in Orbit-Operations and Lessons Learned. In: *The 18th Annual AIAA/USU Conference on Small Satellites*, Logan, Utah, USA.